Physics of Fluids

Transport dynamics of an ellipsoidal particle in free molecular gas flow regime

Cite as: Phys. Fluids **31**, 037104 (2019); https://doi.org/10.1063/1.5081074
Submitted: 13 November 2018 . Accepted: 18 February 2019 . Published Online: 12 March 2019

Arun K. Chinnappan, Rakesh Kumar, Vaibhav K. Arghode, and Rho Shin Myong

Transport dynamics of an ellipsoidal particle in free molecular gas flow regime

Cite as: Phys. Fluids 31, 037104 (2019); doi: 10.1063/1.5081074
Submitted: 13 November 2018 • Accepted: 18 February 2019 •
Published Online: 12 March 2019

Arun K. Chinnappan,[1,a)] Rakesh Kumar,[1,b)] Vaibhav K. Arghode,[1,c)] and Rho Shin Myong[2,d)]

AFFILIATIONS

[1] Department of Aerospace Engineering, Indian Institute of Technology Kanpur, Kanpur Nagar, Uttar Pradesh 208016, India
[2] Department of Aerospace and Software Engineering, Gyeongsang National University, Jinju, Gyeongnam 52828, South Korea

[a)] Graduate Student.
[b)] Associate Professor. **Author to whom correspondence should be addressed:** rkm@iitk.ac.in. **Telephone:** +91-9411396999 and +91-5122596301.
[c)] Assistant Professor.
[d)] Professor.

ABSTRACT

Translational and rotational dynamics of a transporting particle in the free molecular gas flow regime are investigated using an in-house, multi-species, three dimensional Direct Simulation Monte Carlo (DSMC) solver. The DSMC algorithm is modified to study free molecular gas flows and validated against the analytical results for the dynamics of a spherical particle. A particular focus of this work is on estimating the effects of particle size, shape, and orientation on the dynamics of an ellipsoidal particle in free molecular gas and comparing them with that of a spherical particle. Properties such as particle speed, temperature, drag, and heat transfer coefficients are considered for comparison. The effect of particle shape on the aforesaid properties is qualitatively discussed and quantified through a comprehensive analysis taking care of lift, pitching moment, particle rotation, and the associated resistive torque. The relaxation of an ellipsoidal particle to surrounding gas conditions is simulated at zero and non-zero angles of attack to demonstrate the effect of particle orientation. Furthermore, the particle size effect on its translational and rotational dynamics is discussed. Finally, the trajectory of a spherical particle is compared with that of an ellipsoidal particle at different eccentricities.

I. INTRODUCTION

Multiphase flows including gas and granular particle phases have many applications in industries such as cyclone separators, sand blasting, sand storm, and pollution control systems and in specific operations such as planetary landing, high speed flight of a fighter aircraft through a sand storm, and rain clouds. Numerous studies have been done in several years to study gas-granular flow behavior. However, most of its applications are limited to the low-speed and continuum regime. Interestingly, not many studies are found in the high speed and free molecular flow regime considering gas-granular flows although it is important to study the gas-granular flow characteristics in order to address several practical situations such as unburned fuel in solid propellant rocket nozzles and dust dispersion in lunar/planetary landings. Experimental studies are quite expensive in order to mimic low density environments as well as high speed flows. Moreover, the conventional Navier-Stokes solver is not suitable because of continuum failure at the free molecular/transitional regime, such as those found in lunar landing, where the characteristic length is comparable to the mean free path of a gas molecule. Many researchers have proposed theoretical approaches to study gas-granular flows at the free molecular regime, notably: Epstein[1] derived a kinetic theory based drag relation for a low speed spherical particle translating in a Maxwellian gas environment. This work was extended by Baines[2] for any particle velocity in the case of specular reflections. Sauer[3] derived an analytical relation to determine total heat transfer experienced by a particle in the free molecular regime. Gallis *et al.*[4] proposed a theoretical relation using Green's function approach to calculate drag and heat flux experienced by a particle moving in the free molecular regime for monatomic gas. This theoretical relation was extended to di-atomic gas by incorporating rotational and vibrational effects by Burt[5] and used to study the effects of unburned solid propellants in rocket nozzles. In the work reported by Morris *et al.*,[6] the aforementioned relation was used to predict the flow and dust emission mechanism of lunar sand particles due to plume impingement from the nozzle. There are other notable studies in order to predict drag in rarefied/free molecular regimes.[7–9]

All the aforementioned studies have considered particles as perfect spheres so as to make the problem tractable in the theoretical framework albeit the simplification was brought about at the cost of accuracy. Numerous studies were performed in order to derive aerodynamic coefficients for non-spherical particles in the continuum regime,[10,11] and several complexities were reported. A single characteristic parameter (diameter) is enough to describe the behavior of a sphere, whereas at least two parameters are required to study even for regular non-spherical particles, such as ellipsoids. Moreover, the pitching torque and lift force need to be considered if the angle of attack is non-zero. The tracing/tracking of ellipsoidal particles is quite complicated because of the addition of dynamic equations, which need to be solved along with fluid flow equations. Jeffery[12] analytically derived torque components acting along the principal axes of ellipsoidal particles in creeping viscous fluid. This theory was proved through an experimental study by considering an aluminum ellipsoidal particle immersed in water-glass fluid.[13] Brenner[14–18] extended this analytical work to study arbitrary particle motion under Stokes flow conditions. Mortensen *et al.*[19] studied the dynamics of ellipsoidal particles in turbulent flow using direct numerical simulations (DNSs) without considering the effects of particles on gas. Similar kinds of experimental and numerical studies were performed to study non-spherical particle dynamics/behavior in turbulent flows.[20–22]

Noteworthy is the fact that all of these studies are restricted to the continuum regime and carried out considering only the aerodynamics perspective. To this end, the current work aims to study the importance of particle shape consideration in the free molecular regime, with its effect on both aerodynamics and heat transfer aspects. In this work, we have modified and used an in-house kinetic-particle based Direct Simulation Monte Carlo (DSMC) solver to study particle behavior in the free molecular regime. The effect of particle shape is studied from the standpoint of particle's relaxation with the freestream gas flow. The results are compared with the theory in terms of particle properties such as velocity and temperature and surface properties such as drag and heat transfer coefficients. However, a detailed discussion about the dynamics of an ellipsoidal particle has not been attempted at this stage.

This paper is arranged as follows: a brief description of the DSMC method and modifications to reduce computational cost is given in Sec. II, and the validation cases for this proposed method are presented in Sec. III. Section IV explains the numerical procedures to study the ellipsoidal particle and its effect on the free molecular regime, and this is followed by conclusions in Sec. VI.

II. COMPUTATIONAL MODEL: THE DSMC METHOD

The Direct Simulation Monte Carlo method (DSMC) is a particle-based method proposed by Bird for the simulation of non-equilibrium gas flows.[23] The method deals with simulated molecules, each of which represents a large number of real molecules. The method governs the physics through molecular movements and collisions. For a given time step, molecules are moved with their velocities. Molecular collisions are modeled probabilistically. The macroscopic parameters are calculated by time averaging the sampled data. The DSMC method does not produce a direct solution to the Boltzmann equation, but it evaluates the same

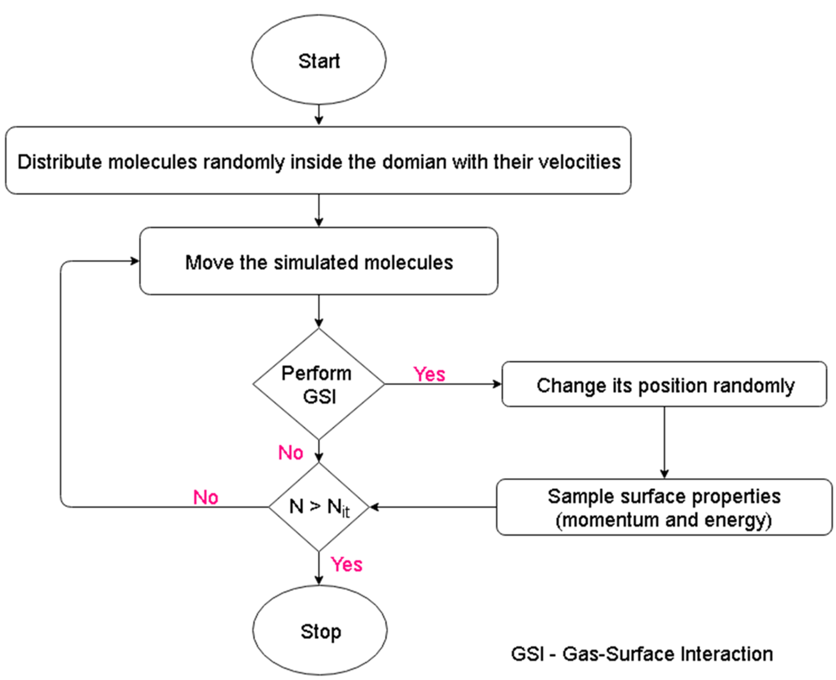

FIG. 1. Modified DSMC algorithm.

physics as the Boltzmann equation, and it has been demonstrated that the DSMC solution approaches the solution of the Boltzmann equation in the limit of vanishing cell size and time step.[23] The detailed explanation of the method can be found in Refs. 23 and 24. The parallel, in-house, multi-species, DSMC solver named Non-equilibrium Flow Solver (NFS) used in this work was developed recently based on Bird's methodology and validated against several experimental and other numerical studies.[25,26] In our solver, the Variable Hard Sphere (VHS) model is used for elastic collisions. The quantum and continuous versions of the Larsen-Borgnakke model are employed to model inelastic collisions. Both Maxwell[27] and Cercignani-Lampis-Lord (CLL)[28] models were implemented to study gas-surface interactions.

To study the problem at hand, which involves flow of argon over a non-spherical particle in the free molecular regime, we have modified the DSMC algorithm to reduce computational cost. In the first place, gas-gas collisions are not modeled in the modified DSMC algorithm consistent with the assumptions involved in the free molecular regime. Furthermore, in the free molecular flow regime, it is reasonable to neglect the effect of reflected particles on the incident gas stream, as far as effects on body are concerned. Therefore, to ensure this, we have made appropriate modifications to the gas-surface interactions in the DSMC algorithm. Once a molecule hits the particle surface, the molecular velocity is made to remain unchanged, and it is relocated randomly inside the domain. In other words, the incident gas flow is assumed to be unaffected by the presence of body, which is a valid assumption in the free molecular regime.[29] However, the incident and reflected momentum/energy of gas molecules during gas-surface collision is sampled to calculate forces, moments, and heat flux experienced by the particle. Thus, the actual gas-surface interaction is modeled, but post-reflection velocities are not assigned to the gas molecules to ensure that gas properties are constant throughout the simulation, implying that the proposed model is one-way coupled. Moreover, the computational grid is not used in this work since the only purpose of a grid in the DSMC method is to perform gas-gas collisions and sampling gas properties, which are neglected in the present work. The flowchart of this algorithm is shown in Fig. 1.

III. SOLVER VALIDATION

The modified DSMC solver for modeling free molecular gas flows is validated for flow over a sphere and that over a flat plate. The surface properties such as drag, lift, and heat transfer are compared with available analytical results. Three case studies are carried out in this section, viz., the first case study involves flow over a spherical particle at different speed ratios, while flow over a flat plate is simulated in the second study. In the third case study, spherical particle relaxation is simulated at a very low speed ratio.

A. Flow over a spherical particle in free molecular regime

A cubical computational domain of size 10 μm is considered with a spherical particle at the center. Argon is used as the gas species. The gas density and temperature are taken as 1.989×10^{-5} kg/m^3 and 500 K, respectively. The bulk velocity of gas is varied based on the speed ratio, which is the ratio of the particle speed to the mean molecular speed of gas ($S = \frac{U}{\sqrt{2RT}}$). The particle volume is taken as 5.236×10^{-19} m^3, which represents the volume of a sphere of diameter 1 μm. The mass of the particle is 9.94×10^{-16} kg. The particle temperature is the same as that of gas. The time step is taken as 1×10^{-9} s for all simulations, which is much smaller than the mean collision time of the gas. Each simulation is performed with 20 000 simulated molecules with 50 000 samples. The periodic boundary condition is employed at all six sides of the domain. The CLL model[28] is used for gas-surface interaction with an accommodation coefficient of unity, corresponding to diffuse reflection with full thermal accommodation.

It was found by several researchers that particle drag and heat flux coefficients depend only on the molecular speed ratio, S, in the free molecular regime.[29,30] The analytical relationship for the heat transfer rate experienced by a spherical particle[3] is expressed in terms of the thermal recovery factor r' and modified Stanton number St$'$ as

$$r' = \frac{(2S^2+1)\left[1+\dfrac{\mathrm{ierfc}(S)}{S}\right]+\dfrac{2S^2-1}{2S^2}\mathrm{erf}(S)}{S^2\left[1+\dfrac{\mathrm{ierfc}(S)}{S}\right]+\dfrac{\mathrm{erf}(S)}{2S^2}}, \tag{1}$$

$$\mathrm{St}' = \frac{S^2 + S\,\mathrm{ierfc}(S) + \dfrac{\mathrm{erf}(S)}{2}}{8S^2}, \tag{2}$$

where ierfc(S) is the integrated complementary error function.

The analytical relationship for the drag coefficient of a spherical particle in the free molecular limit[29] is given by

$$C_D = \frac{e^{-S^2}}{\sqrt{\pi}S^3}(1+2S^2) + \frac{4S^4+4S^2-1}{2S^4}\,\mathrm{erf}(S) + \frac{2\sqrt{\pi}}{3S_{\mathrm{p}}}, \tag{3}$$

where S_{p} is the speed ratio corresponding to the particle temperature, $S_{\mathrm{p}} = \frac{U}{\sqrt{2RT_{\mathrm{p}}}}$. In the present case, $S_{\mathrm{p}} = S$ since the particle and gas temperature are the same. In DSMC simulations, the modified Stanton number is derived from heat flux Q and is given by

$$\mathrm{St}' = \frac{Q}{A\rho U c_p (T_{\mathrm{r}} - T_{\mathrm{w}})}\frac{\gamma}{\gamma+1}, \tag{4}$$

where A is the surface area of a spherical particle, ρ is the free stream gas density, c_p is the specific heat capacity of gas at constant pressure, T_{r} is recovery temperature, and T_{p} is the particle temperature, which is the same as the gas temperature in the current case. The analytical equation (1) is used in DSMC simulations to find the recovery factor, while the recovery temperature can be obtained from Eq. (5), given by Oppenheim,[30]

$$T_{\mathrm{r}} = T_\infty + \frac{r'(T_0 - T_\infty)\gamma}{\gamma+1}. \tag{5}$$

The variation of the drag coefficient and modified Stanton number with respect to the speed ratio for a spherical particle is plotted and compared with analytical results given by (2) and (3) in Fig. 2. The results obtained from our in-house 3D DSMC solver

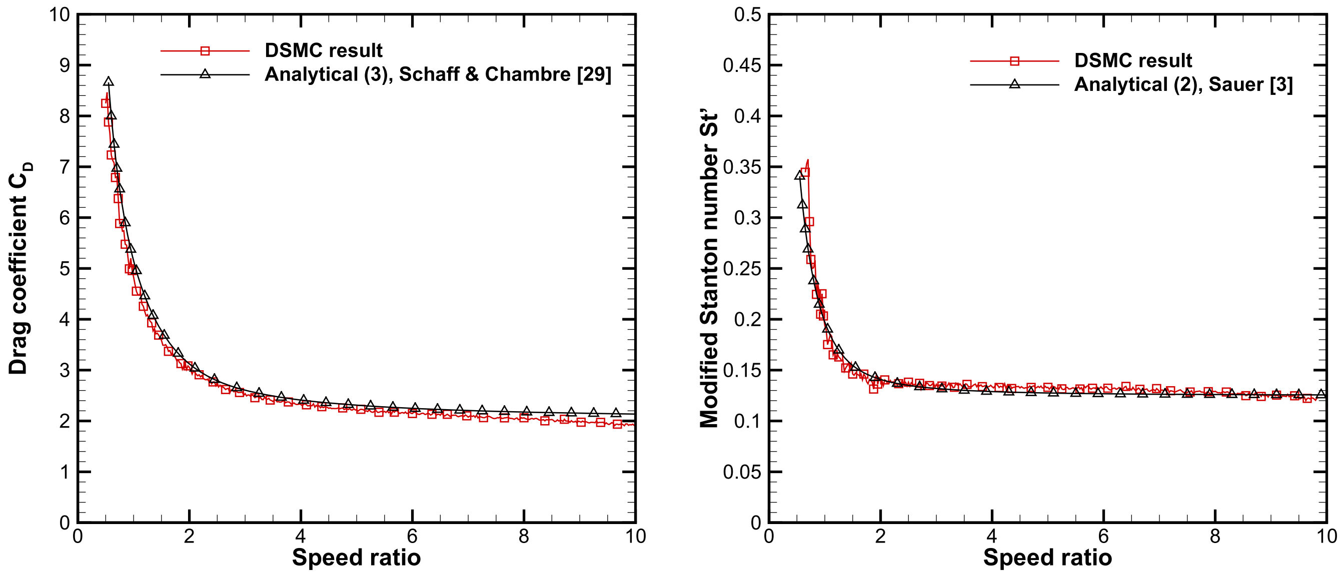

(a) (b)

FIG. 2. Comparison of DSMC results with analytical results for a spherical particle. (a) Drag coefficient and (b) modified Stanton number.

are found to be in good agreement with the analytical results for all speed ratios analyzed in this work.

B. Flow over a flat plate in free molecular regime

Now we consider flow over a flat plate at a finite angle of attack in the free molecular regime with an aim to validate the computational framework for the calculation of lift and drag forces over an object. The flat plate is chosen as the representative object so as to compare the data with theory. The problem involves free molecular flow of argon over a flat plate at different angles of attack. The length of the flat plate is considered to be 2 μm with an aspect ratio of 40. By considering the very small thickness of the flat plate and to model accurate gas-surface interactions, the time step for this simulation is considered to be 4×10^{-12} s. Each case is simulated with 10 000 simulated molecules with 200 000 samples. This simulation is performed at a speed ratio of 2, and the angle of attack is varied from 0 to π. All other flow parameters are the same as that of the previous case. The analytical relation[29] for lift and drag coefficients with the assumption of uniform surface temperature is given by

$$C_L = \frac{\cos\theta}{S^2}\left[\operatorname{erf}(S\sin\theta) + \sqrt{\pi}\frac{S^2\sin\theta}{S_p}\right], \tag{6}$$

$$C_D = \frac{2}{\sqrt{\pi}S}\Bigg[e^{-(S\sin\theta)^2} + \sqrt{\pi}S\sin\theta\left(1+\frac{1}{2S^2}\right)\operatorname{erf}(S\sin\theta) + \frac{\pi S}{2}S_p\sin^2\theta\Bigg]. \tag{7}$$

In DSMC simulations, the drag and lift coefficients are obtained from drag and lift force as

$$C_L = \frac{L}{\frac{1}{2}\rho U^2 A}, \tag{8}$$

$$C_D = \frac{D}{\frac{1}{2}\rho U^2 A}, \tag{9}$$

where L and D are lift and drag forces, respectively. The variation of the lift to drag ratio for different angles of attack obtained from DSMC simulations is compared with the analytical results in Fig. 3.

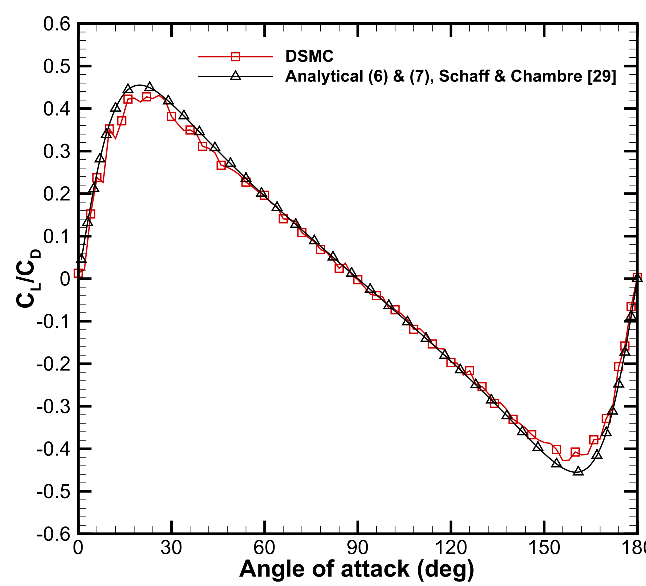

FIG. 3. Comparison of DSMC results with analytical results for a flat plate.

It is found that DSMC simulation results are in good agreement with the analytical result and the maximum error is less than 5%.

C. Spherical particle relaxation to gas at low speed ratio

In this section, a temporal homogeneous test case is simulated and the results are examined for gas flow over a spherical particle. The flow chart for this algorithm is presented in Fig. 4. The procedure involves the initialization of particle velocity and temperature, followed by the simulation of the modified DSMC algorithm in a particle frame, which implies relative gas flow over a particle at constant gas temperature. The relative gas velocity and particle temperature are updated by considering gas-surface interactions. This procedure is repeated until the relative velocity and difference in gas and particle temperature approximately reach zero.

The initial particle velocity and temperature are taken as 500 m/s and 100 K, respectively. Argon is used as gas species with a velocity of 600 m/s and at a temperature of 1514 K. The gas number density is considered as 3×10^{20} (1/m^3), which corresponds to the Knudsen number (Kn) of 4314 using particle diameter as the reference length. The number of simulated molecules and time step are taken as 20 000 and 1×10^{-10} s, respectively. The particle temperature and velocity are updated for every 1×10^{-4} s. The unsteady simulation is performed until the physical time reaches 2 s. The temporal variation of particle velocity, temperature, and heat flux is compared with the analytical relationships. The analytical relation for drag in the low speed ratio limit[1] and the corresponding heat flux expression derived by Gallis *et al.*[4] are given below:

$$\vec{F}_{\text{Epstein}} = -(\rho c_0^2 \pi R_p^2)\left[\frac{8}{\sqrt{\pi}} + (1-\sigma)\sqrt{\frac{\pi T_p}{T}}\right]\frac{\vec{V}_p}{3c_0}, \tag{10}$$

$$Q_{\text{Epstein}} = \rho c_0^3 \pi R_p^2 (1-\sigma)\left[\frac{2}{\sqrt{\pi}} - \frac{T_p}{T}\frac{2}{\sqrt{\pi}}\right], \tag{11}$$

where σ is the fraction of molecules undergoing specular reflection ($\sigma = 0$ in this case), ρ is the density of gas, c_0 is the most probable speed of gas, R_p is the radius of the particle, $\vec{V}_p$ is the particle velocity, and T_p and T_g are particle and gas temperatures, respectively.

The velocity and temperature of the particle are updated (to the first order approximation) using drag and heat flux as follows:

$$\vec{V}_p^{t+1} = \vec{V}_p^{t} + \frac{\vec{F}\Delta t}{m_p}, \tag{12}$$

$$T_p^{t+1} = T_p^{t} + \frac{Q\Delta t}{m_p c_{p_p}}, \tag{13}$$

where c_{p_p} is the specific heat capacity of the particle.

Figure 5 shows the comparison of particle temperature, velocity, and normalized heat flux with the corresponding analytical solutions. The particle velocity and temperature are found to be in good agreement with the theoretical data. At the same time, the normalized heat flux is found to be in good agreement with the analytical data obtained from Eq. (11). The maximum error is found to be less than 1%, thus showing fairly good agreement with the theoretical predictions. Furthermore, it is interesting to note that in the free molecular regime, the freestream gas molecules impinge on the wall without colliding with other gas molecules by virtue of free molecular assumption. Due to this effect, the efficiency of heat transfer increases with the Knudsen number. Thus, the upper limit of normalized heat transfer coefficient is always in the free molecular regime.

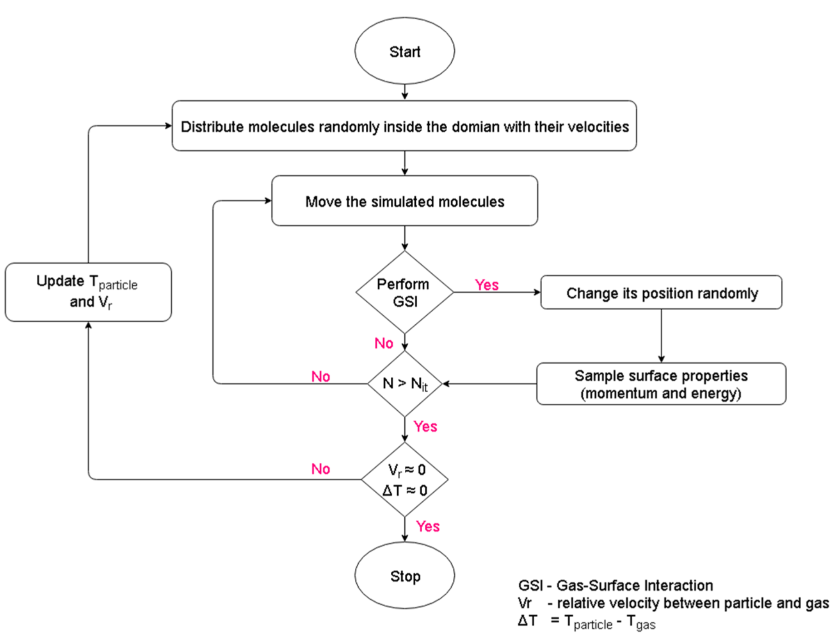

FIG. 4. Particle relaxation.

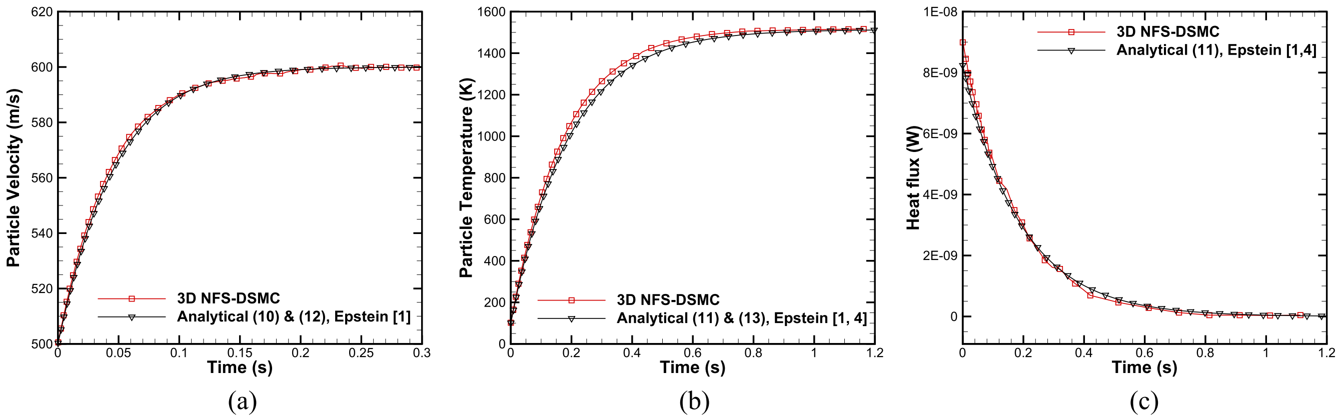

FIG. 5. Comparison of DSMC results with analytical solutions for a spherical particle. (a) Particle velocity, (b) particle temperature, and (c) particle heat flux.

IV. DYNAMICS OF ELLIPSOIDAL PARTICLES IN FREE MOLECULAR REGIME

To study shape effects, we have considered prolate ellipsoidal particles having the same volume as that of the sphere of 1 μm diameter. In this study, there are four different ellipsoidal shapes considered with eccentricities of 0.3, 0.5, 0.7, and 0.9.

A. Coordinate system

To model the dynamics of a non-spherical particle, it is convenient to have two Cartesian coordinate systems. The inertial frame $\boldsymbol{x} = [x, y, z]$, which is the fixed frame of reference. The particle frame $\boldsymbol{x}' = [x', y', z']$ has an origin at the center of mass of the particle and axes aligned with the principal axes of the particle. The different reference frames are shown in Fig. 6.

In the first stage of the model development discussed in this work, we consider angular motion only about the lateral axis, z', while angular motions about the other two axes are assumed to be negligible. This assumption is also valid since there is no lateral/transverse bulk motion of fluid considered in this work. The transformation from the particle reference frame to the inertial frame can be obtained by using the Euler transformation as $\vec{x} = R \cdot \vec{x}'$, where R is the rotational matrix and θ is the pitching angle, as shown in Fig. 6,

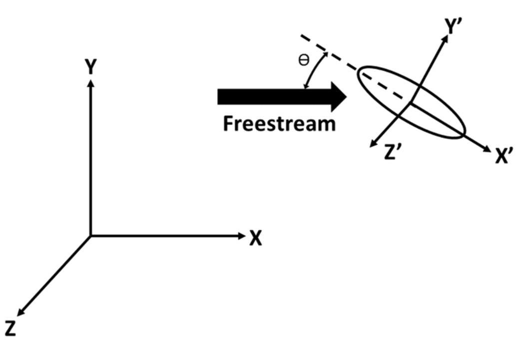

FIG. 6. Coordinate system: inertial frame $\boldsymbol{x}$ and particle frame $\boldsymbol{x}'$.

$$R = \begin{bmatrix} \cos\theta & \sin\theta & 0 \\ \sin\theta & \cos\theta & 0 \\ 0 & 0 & 1 \end{bmatrix}. \tag{14}$$

B. Equations of motion

The equations of motion of a non-spherical body can be decoupled into translational and rotational modes, which are written in inertial and particle axis frames, respectively, below.[31]

Translational motion:

$$m_p \frac{d\vec{V}_p}{dt} = \vec{F}, \tag{15}$$

where m_p is the mass of a particle, $\vec{V}_p = [v_x, v_y, v_z]$ is the translational velocity vector, and $\vec{F} = [F_x, F_y, F_z]$ is the force vector acting on a particle in the inertial reference frame.

Rotational motion (without considering ω_x' and ω_y'):

$$I_z' \frac{d\omega_z'}{dt} = T_z', \tag{16}$$

where $\vec{\omega}' = [0, 0, \omega_z']$ is the angular velocity vector of a particle about its principal axes. I_z' is the moment of inertia with respect to the particle's z' axis, which can be expressed as, $I_z' = \frac{m_p(a^2+b^2)}{5}$, where a is the semi-major axis and b is the semi-minor axis of the ellipsoidal particle. T_z' is the torque acting on a particle about its z' axis.

The procedure involves solving the flow over an ellipsoidal particle in the particle reference frame using the in-house modified DSMC solver to obtain force vector, torque, and heat flux. The force vector is then transformed to the inertial reference frame using the Euler transformation. The force vector (in the inertial frame) and torque (in the particle frame) can then be used to solve for $\vec{V}_p$ and $\vec{\omega}'$ using Eqs. (15) and (16), respectively. Finally, the particle velocity, orientation, and temperature are updated.

There are two contributions to torque in Eq. (16). The first one, $\vec{T}'_{\mathrm{off}}$, is caused by the finite lift and offset of the center of pressure from the center of mass. Hence, it can be expressed as $\vec{T}'_{\mathrm{off}} = \delta\vec{x}'_{cp} \times \vec{F}'$, where $\delta\vec{x}'_{cp}$ is the position vector from the center of mass to the center of pressure, and $\vec{F}'$ is the resultant force vector in the body axis system, as shown in Fig. 7. Noteworthy is the fact

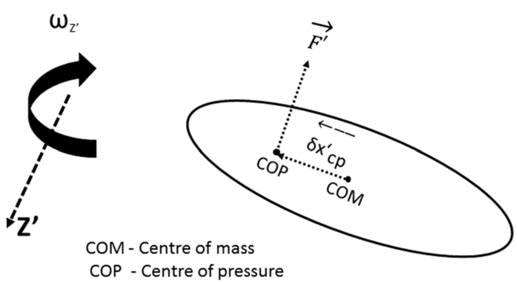

FIG. 7. Schematic figure for the evaluation of offset torque.

that the particle does not experience a torque at zero angle of attack because of the zero lift even though the center of pressure is ahead of the center of mass. In this case, we have considered only pitching torque $T'_{\text{off-z}}$ (rotation with respect to z' axis) and other two components are negligible, as discussed in Sec. IV A. The force vector is obtained by sampling the incident/reflected momentum of the gas molecules interacting with the surface.

The variation of the location of center of pressure, calculated using the DSMC analysis, with respect to angle of attack for an ellipsoidal particle of eccentricity 0.9 (which is close to a cylindrical shape) is compared with the approximated expressions for cylindrical particles from the literature[32–34] in Fig. 8. The expressions from Rosendahl[32,33] and Yin *et al.*[34] are given in the following equations:

$$\frac{x_{cp}}{L} = 0.25(1 - \sin^3 \theta), \tag{17}$$

$$\frac{x_{cp}}{L} = 0.25 \cos^3 \theta. \tag{18}$$

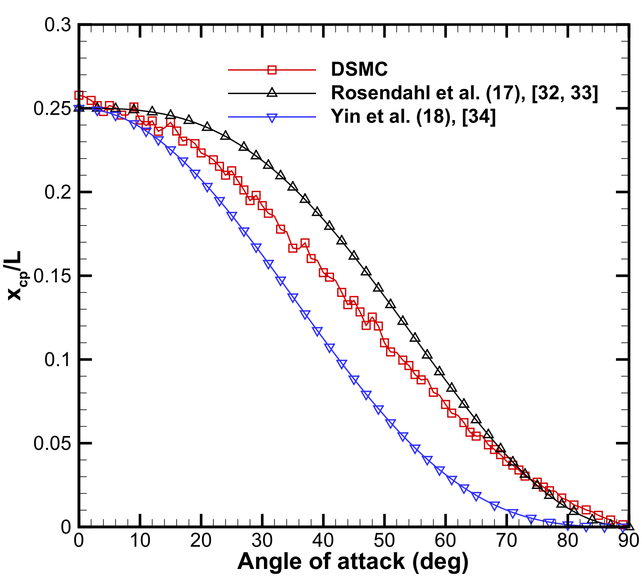

FIG. 8. Comparison of the location of the center of pressure with respect to the angle of attack.

The shown location of the center of pressure x_{cp} is measured from the leading edge of the particle and normalized with the length of the ellipsoidal particle. It is evident from Fig. 8 that the variation of the centre of pressure as obtained from our DSMC results is qualitatively in fair agreement with the expressions given by Rosendahl[32,33] and Yin *et al.*[34]

The second contribution to torque is the resistance caused by the fluid on a rotating particle. If a particle rotates at an angular velocity of ω'_z, it creates a torque in the opposite direction due to friction. In other words, every cross section of an ellipsoid experiences a drag and its cumulative effect is the torque, which opposes the particle motion, as depicted schematically in Fig. 9.

If F'_{res} is the force acting on an ellipsoidal cross section, which varies along the longitudinal axis and is at a distance of r from the center of rotation, then the resistive torque can be written as

$$T'_{\text{res}} = 2 \int_0^a F'_{\text{res}} r dr. \tag{19}$$

The resistive force is given as $F'_{\text{res}} = \frac{1}{2}\rho(r\omega'_z)^2 c_d A_c$, where ρ is the local air density, which is the same as the free stream density, and c_d is the drag coefficient for cross-sectional area A_c and varies along the longitudinal axis due to change in the local linear velocity. The cross-sectional area of the ellipsoidal element is a circular cylinder, whose magnitude can be written using the equation of an ellipse as $A_c = \frac{2b}{a}\sqrt{a^2 - r^2}$, as shown in Fig. 9. A similar kind of approach was followed to derive resistive torque for cylinder particle movement in continuum flows.[32,34] Noteworthy is the fact that the resistive torque is always opposite to offset torque $T'_{\text{off-z}}$.

The speed ratio, S, across the longitudinal cross section is very small since the semi-major axis a is in the order of 10^{-7} m and the local linear velocity varies along the longitudinal axis as $U_{\text{local}} = r\omega'$. Now, for $S \to 0$, the drag coefficient for free molecular flow over a cylindrical body[29] gets reduced to $c_d = \frac{\pi^{\frac{3}{2}} c_{0\text{p}}}{4(r\omega'_z)}$, where $c_{0\text{p}} = \sqrt{2RT_{\text{p}}}$ is the most probable speed corresponding to the particle temperature T_{p}, r is the longitudinal distance from the center of an ellipsoid, and ω'_z is the angular velocity of the particle about the lateral axis. Therefore, the resistive torque can be written as

$$T'_{\text{res}} = \frac{b}{2a}\rho\omega'_z \pi^{\frac{3}{2}} c_{0\text{p}} \int_0^a r^2\sqrt{a^2 - r^2} dr = \frac{ba^3}{32}\rho\omega'_z \pi^{\frac{5}{2}} c_{0\text{p}}. \tag{20}$$

C. Particle relaxation at zero angle of attack

Now we consider the relaxation of a non-spherical particle at zero angle of attack to freestream gas. For this study, we have considered four ellipsoidal particles with eccentricities of 0.3, 0.5, 0.7, and 0.9, while the particles have the same volume as that of a sphere of 1 μm diameter. We have compared the results with those obtained for flow over a spherical particle. Every particle movement is considered to be a separate simulation, and the procedure is shown in Fig. 4. In this case, we have considered an initial particle velocity of 500 m/s with an initial temperature value of 100 K. The background gas is kept stagnant at a temperature of 100 K. All other numerical parameters are the same as mentioned in Sec. III C.

The temporal variation of particle speed (U_p) and temperature (T_{p}) is shown in Fig. 10. The time on the x-axis is normalized with

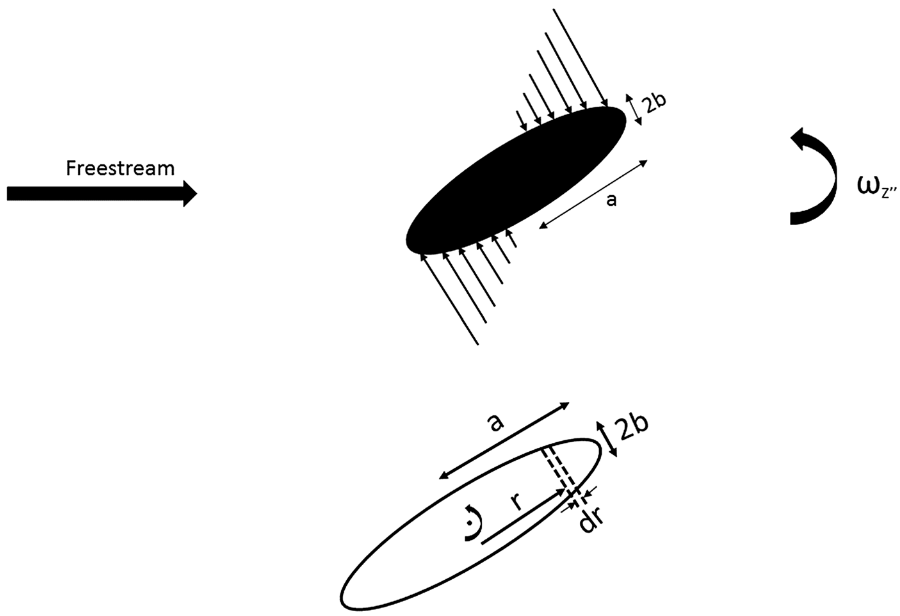

FIG. 9. Schematic figure for the evaluation of resistive torque (the arrows in the figure represent the relative flow velocity due to particle rotation).

the relaxation time for a sphere based on the slip-corrected Stokes equation, i.e., $\tau = \frac{m_p C}{3\pi\mu D_p}$, where μ is the dynamic viscosity, D_p is the diameter of a spherical particle, and C is the slip correction factor. Millikan's slip correction factor[35] is used in this work, which is $C = 1 + (0.864 + 0.29e^{\frac{-1.25}{\mathrm{Kn}}})\mathrm{Kn}$. The particle speed and temperature on the y-axes are normalized with the initial particle velocity, U_{initial}, and initial particle temperature, T_{initial}, respectively. It is observed that the relaxation time increases with eccentricity for both velocity and temperature. As eccentricity increases, the particle becomes slender. In other words, since the angle of attack is zero, the contact surface area decreases as eccentricity increases. Therefore, less number of gas-surface collisions occurs as eccentricity increases, which makes less momentum and energy imparted to the surface for ellipsoidal particles as compared to sphere. Due to this effect, the

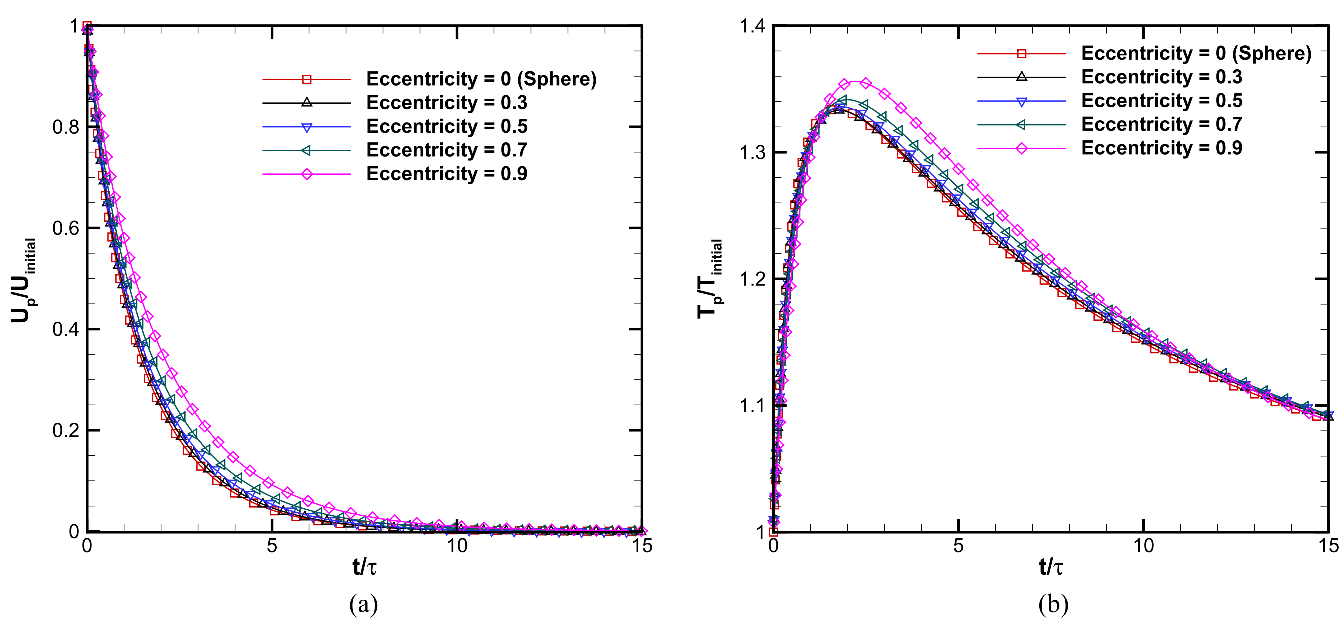

FIG. 10. Comparison of relaxation of spherical particle vis-a-vis ellipsoidal particle of different eccentricities at zero angle of attack (m_p = 9.958 × 10^{-16} kg). (a) Particle speed and (b) particle temperature.

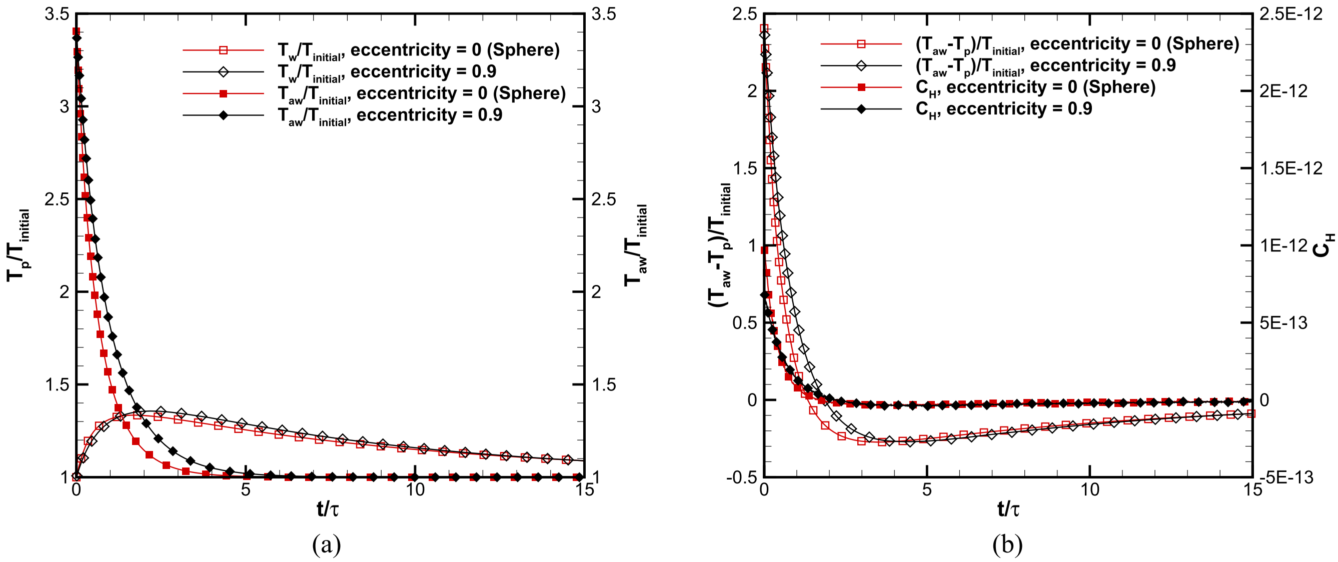

FIG. 11. Comparison of the normalized variation of particle temperature, T_p, adiabatic wall temperature, T_{aw}, and normalized heat flux, Q, of a spherical particle with an ellipsoidal particle of eccentricity 0.9 at zero angle of attack (m_p = 9.958 × 10^{-16} kg). (a) T_{aw} and T_p (both normalized). (b) $T_{aw} - T_p$ and Q (both normalized).

velocity and temperature relaxation time increase with increasing eccentricity at zero angle of attack.

The variation of normalized particle temperature, adiabatic wall temperature, and particle heat transfer rate with respect to normalized time for a sphere and an ellipsoidal particle of eccentricity 0.9 is plotted in Fig. 11. This explains the variation of particle temperature with respect to time, as shown in Fig. 10. The temperatures are normalized with initial particle temperature, while the heat transfer rate of the particle is normalized as $C_H = \frac{Q}{\frac{1}{2}\rho U^3_{initial}}$, wherein the convective heat transfer rate, Q, of the particle is given as

$$Q = A\rho U_p c_p (T_{aw} - T_p)\mathrm{St}, \tag{21}$$

where St is the Stanton number and T_{aw} is the adiabatic wall temperature, $T_{aw} = T_\infty(1 + \frac{\gamma}{\gamma-1}S^2)$. Initially, the heat transfer rate is large due to the high particle velocity and significant difference in T_{aw} and T_p, as shown in Fig. 11. However, the particle velocity starts decreasing with time due to the drag experienced by the particle, which in turns decreases the adiabatic wall temperature. Due to the cumulative effect of decreasing particle speed and the difference in adiabatic and particle temperatures, the particle heat flux starts decreasing with time. Therefore, the slope of particle temperature with time starts decreasing with time and reaches a minimum value, when Q reaches zero, i.e., $T_{aw} - T_p = 0$. This is when a particle attains its maximum temperature. Since speed of a spherical particle decays faster as compared to an ellipsoidal particle, as shown in Fig. 10, the time at which a particle attains the maximum temperature increases with the increase in eccentricity.

D. Particle relaxation at non-zero angle of attack

Now we study the previous case with an initial angle of attack of 10°. Due to high initial particle velocity of 500 m/s relative to the gas, the resulting pitching torque is high, which makes the particle rotate at very high angular speed. The large angular velocity limits the time step to update the pitching angle θ and requires 1×10^{-7} s to update particle orientation, which requires 10^7 simulation time steps to achieve 1 physical second. Due to the computational difficulty associated with very small time step, we have introduced another approach merely to reduce computational cost. In the new approach, flow over an ellipsoidal particle is simulated at different speed ratios and angles of attack to calculate lift, drag, torque coefficients, and Stanton number. Thus a database is developed for free molecular flow over an ellipsoidal particle at different speed ratios and angles of attack. This database is then used to compute the forces, heat flux, and torque to calculate the relaxation of a non-spherical particle at a finite angle of attack with comparatively very little computational effort. The procedure is given below:

1. Initialize gas and particle properties.
2. Calculate particle speed ratio and angle of attack.
3. Find C_D, C_L, C_T, and St for the particular speed ratio and angle of attack from the database using the bi-linear interpolation.
4. Calculate lift, drag, torque, and heat flux.
5. Solve translation and rotational equation of motions using Eqs. (15) and (16), respectively.
6. Update velocity, temperature, and orientation of the particle.
7. Return to step 2 if relative velocity is not zero.

Noteworthy is the fact that accuracy of this approach depends strongly on the database. Thus, in order to make the new approach accurate, we have performed a large number of DSMC simulations at different speed ratios and angles of attack. For example, we carried out DSMC simulations for speed ratios ranging from 0.5 to 10 with a difference of 0.1 and for different angles of attack from 0° to 90° with a difference of 2°. Furthermore, since the gradient in coefficients is found to be very high at low speed ratios, as can be seen in Fig. 2, speed ratio difference is considered to be very small

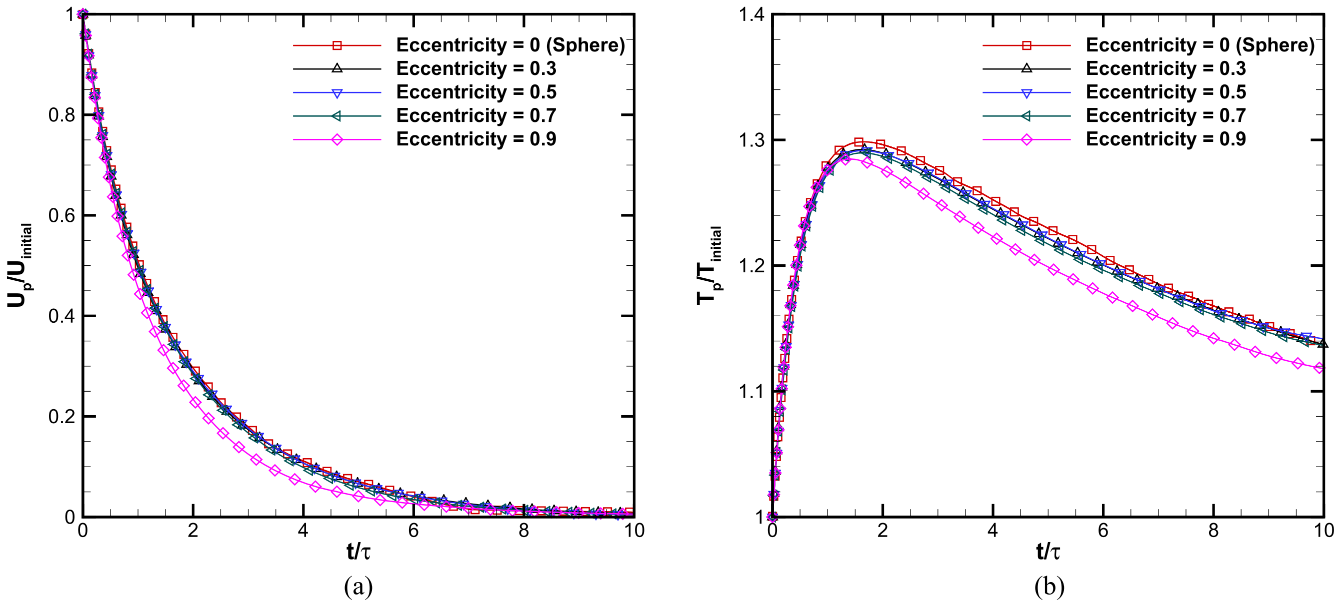

FIG. 12. Comparison of particle relaxation of the sphere with ellipsoidal of different eccentricities (m_p = 9.958 × 10^{-16} kg, and initial angle of attack is 10°). (a) Particle speed and (b) particle temperature.

(ΔS = 0.025) at low speed ratios ranging from 0 to 0.5. Therefore, the total number of simulations for the given free stream conditions turned out to be 5290. This consumed a lot of time, but once the database is generated, the followed approach offers significant savings in effective computational time; the same can be used for further flow calculations associated with the gas-particle combination.

With the aforesaid approach, we have carried out simulations for different ellipsoidal particle shapes (corresponding to different eccentricities) and the results for the variation of speed and temperature of particle with time are shown in Fig. 12. From both variations, the particle relaxation time is found to decrease as particle eccentricity increases, which is opposite to the trends obtained at

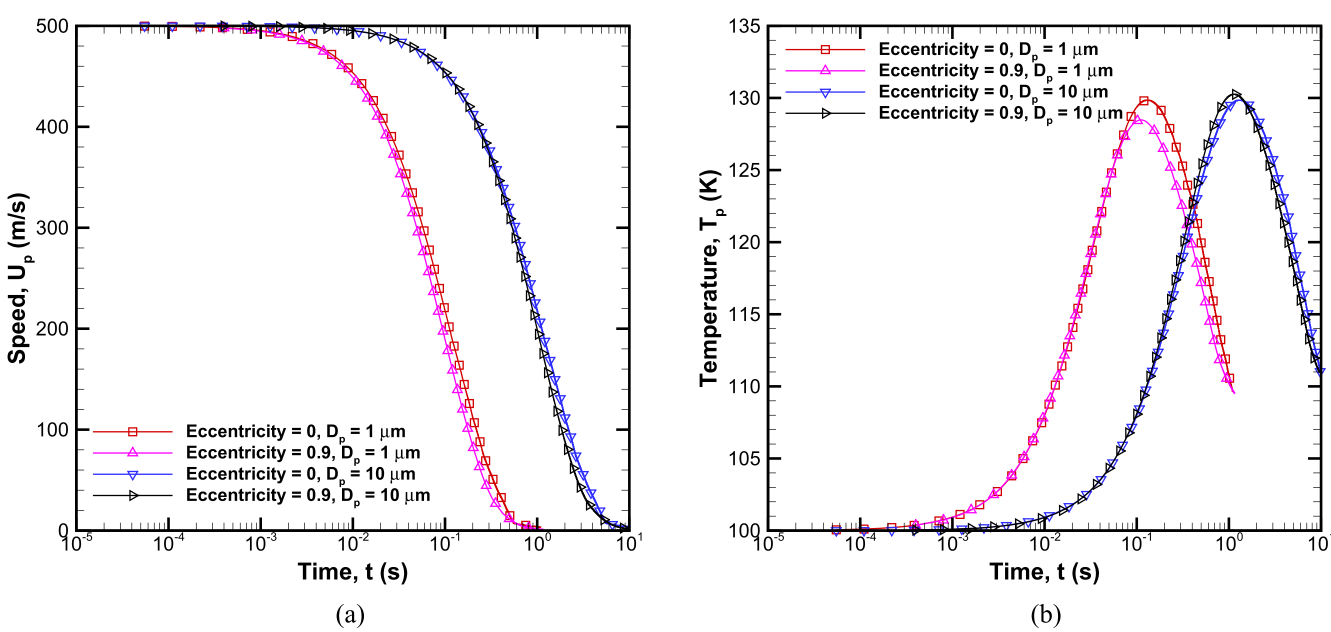

FIG. 13. Comparison of particle relaxation for different sized particles (m_p = 9.958 × 10^{-16} kg and m_p = 9.958 × 10^{-13} kg). (a) Particle speed and (b) particle temperature.

zero angle of attack. This indeed is very interesting. The reason for these trends is explained in Sec. IV D 1 with the help of the angular velocity.

1. Effect of particle size

To study the particle size effect on the relaxation time, we have performed simulations with increased particle size at the same flow conditions mentioned in the previous case. In this case, we have considered a sphere of diameter 10 μm and an ellipsoid with an eccentricity of 0.9 having the same volume as that of a sphere; thus, effectively we have chosen a particle size ten times than that used in the previous case. The density of the particle in all cases is the same as that of previous cases so that the mass is increased by three orders of magnitude $m_p = 9.958 \times 10^{-13}$ kg. The comparison of relaxation for a spherical particle and an ellipsoidal particle is shown along with those corresponding to $d = 1$ μm particle in Fig. 13. It is clear from the figure that the trends for the particle relaxation (in terms of speed and temperature) are the same for two different sized particles. However, interestingly, the relaxation time is found to scale very well with the particle diameter. This can be explained with the help of the Stokes law, according to which the relaxation time is given as $\tau = \frac{m_p C}{3\pi\mu D_p}$, where μ is the dynamic viscosity, D_p is the diameter of the particle, and C is the Millikan slip correction factor, which in turn is given as $C = 1 + (0.864 + 0.29e^{\frac{-1.25}{\mathrm{Kn}}})\mathrm{Kn}$.[35] At a very high Knudsen number (in the free molecular regime, which is considered in this work), the slip correction factor is of the order of Kn ($C \sim$ Kn). Therefore, the relaxation time is theoretically found to scale with the particle diameter by keeping the particle density the same. Thus, our observation regarding the variation of relaxation time with the particle size, as shown in Fig. 13, is consistent with the theory in the free molecular regime. Noteworthy is the fact that the relaxation time varies proportionally to the square of particle diameter in the continuum regime (Kn $\rightarrow$ 0).

In both the abovementioned cases, the relaxation time is found to decrease as eccentricity increases. To explain this phenomenon, the variations of the torque and drag coefficient with respect to the angle of attack at a speed ratio of 3 are presented in Fig. 14. The drag coefficient expression is the same as given in Eq. (9) with the area of cross section the same as that of a sphere of 10 μm, while the expression for the pitching torque coefficient is given as

$$C_T = \frac{T_z}{\frac{1}{2}\rho U^2 \left(\frac{\pi D_p^3}{8}\right)}, \tag{22}$$

where T_z is the pitching torque and D_p is the particle diameter. The fluctuations in the results correspond to the statistical nature associated with the DSMC method. As eccentricity increases, the particle torque increases, as shown in Fig. 14, which makes high eccentricity particles rotate at a very high speed, as shown in Fig. 15. Moreover, the drag coefficient increases as the angle of attack increases, as shown in Fig. 14. Due to this, a high eccentricity particle that is at non-zero angle of attack experiences more torque and rotates at a very high velocity. The cumulative effect of this high angular velocity and a large drag value at a high angle of attack brings the particle to rest in a shorter period of time. The ellipsoidal particles of eccentricity 0.3 to 0.7 are not found to show much deviation from spherical particles because of the small value of torque, while drag is almost constant for all eccentricities and equivalent to that of a sphere. This is the reason why velocity relaxation of ellipsoidal particles of eccentricity 0.3 to 0.7 closely matches with that of a sphere although there is a minor difference observed in temperature relaxation.

From Fig. 15, it is found that large eccentricity particles rotate at higher angular velocities than low eccentricity particles. Moreover,

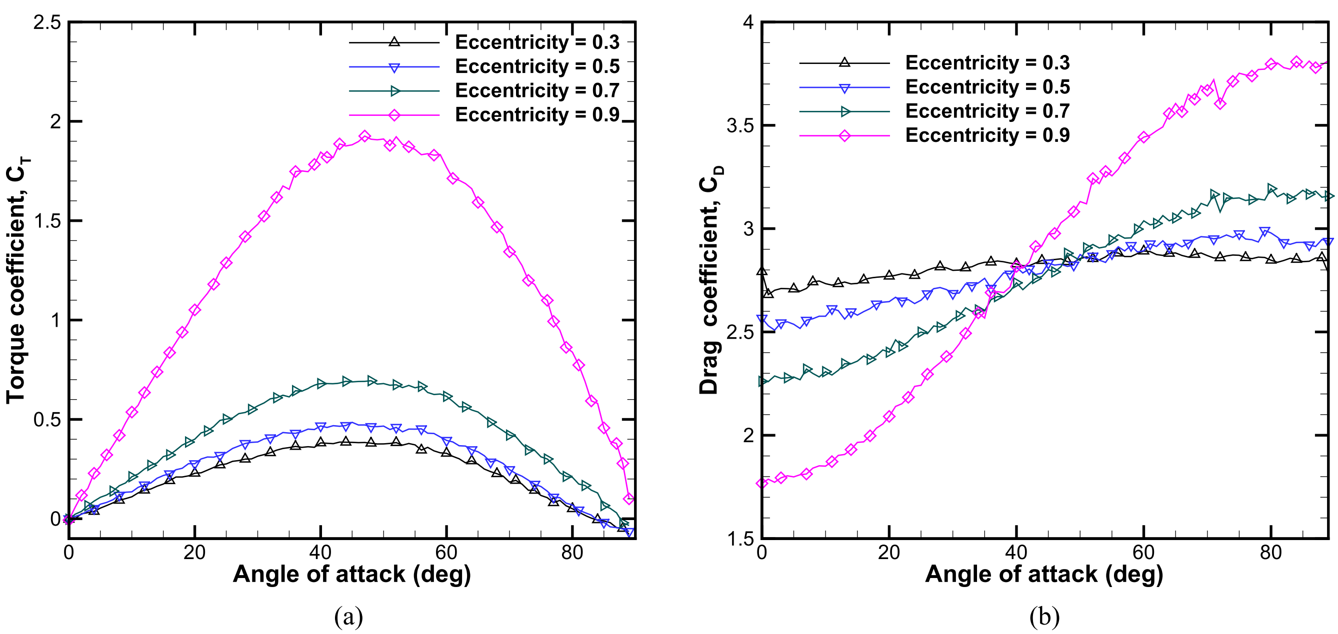

FIG. 14. Variation of torque and drag coefficients at a speed ratio of 3 for different ellipsoidal shapes ($m_p = 9.958 \times 10^{-13}$ kg). (a) Torque coefficient and (b) drag coefficient.

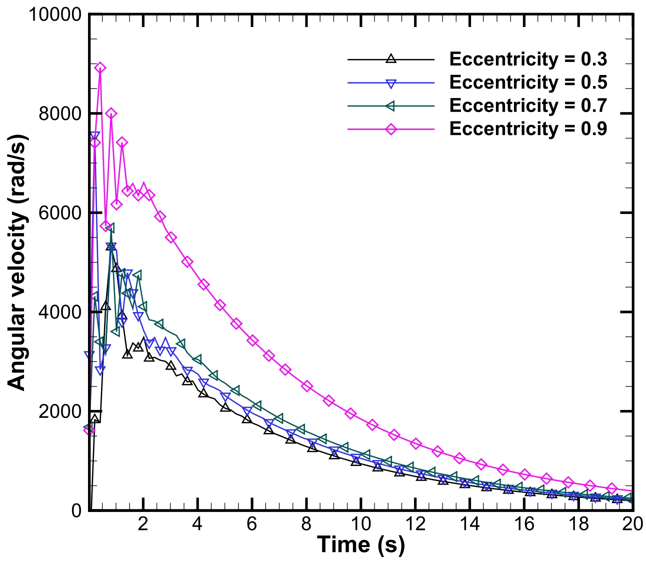

FIG. 15. Comparison of rotational relaxation of the ellipsoidal particle for different eccentricities (m_p = 9.958 × 10^{-13} kg, and initial angle of attack is 10°).

low eccentricity particles reach steady state rotation much more promptly than high eccentricity particles.

2. Comparison with continuum results

It has been found in some studies[36,37] that the drag and torque coefficients increase with the Knudsen number, whereas the lift coefficient decreases. The reason for this contrasting behavior is that the shear stress contribution increases with the Knudsen number, while the contribution due to pressure remains relatively the same.[36] The shear stress contribution favors drag and opposes lift, implying an increase in the drag coefficient and a decrease in the lift coefficient with the increasing Knudsen number.

To verify this effect, we plot in Fig. 16 the variation of drag and lift coefficients with respect to the angle of attack at a speed ratio of 3 for two different eccentricities of 0.7 and 0.9 and at a Knudsen number of 431.4. In this work, we have considered a fully diffuse reflection with complete thermal accommodation at a very high Knudsen number, which makes the lift as well as lift to drag ratio negligible, which is in qualitative agreement with the results available in literature.[23]

In order to make sense of the effect of rarefaction, we have compared the drag and lift coefficients calculated in this work with those obtained in continuum conditions in Fig. 16. The expressions used for calculating the drag and lift coefficients in the Stokes regime (Reynolds number, Re ≪ 1) for an ellipsoidal particle (with eccentricity values of 0.7 and 0.9) have been taken from Refs. 38 and 39 and are written as follows:

$$C_{D,\theta} = C_{D,\theta=0^\circ} + \left(C_{D,\theta=90^\circ} - C_{D,\theta=0^\circ}\right)\sin^2\theta, \tag{23}$$

$$C_{L,\theta} = \left(C_{D,\theta=90^\circ} - C_{D,\theta=0^\circ}\right)\sin\theta\cos\theta. \tag{24}$$

Due to the unavailability of C_D for an ellipsoidal particle at Re = 0.01, we have used the DSMC data for $C_{D,\theta=0^\circ}$ and $C_{D,\theta=90^\circ}$ to obtain the theoretical predictions, as shown in Fig. 16. It is evident from Fig. 16 that the theoretical equations in the Stokes regime given by Eqs. (23) and (24) underpredict the drag coefficient and overpredict the lift coefficient. The difference in the results is due to the increase in shear stress contribution to drag and lift with an increasing Knudsen number and the diffuse wall condition imposed on the surface. For this reason, the effect of lift on the particle dynamics is

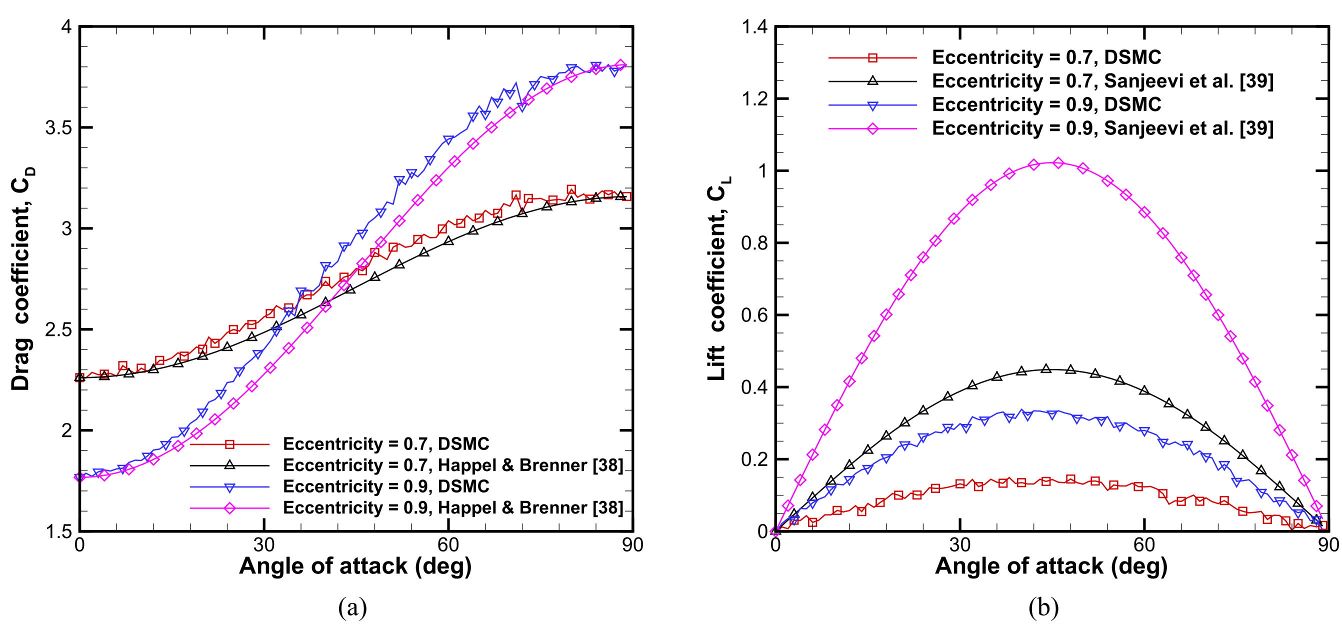

FIG. 16. Variation of lift and drag coefficients at a speed ratio of 3 for different ellipsoidal shapes. (a) Drag coefficient and (b) lift coefficient.

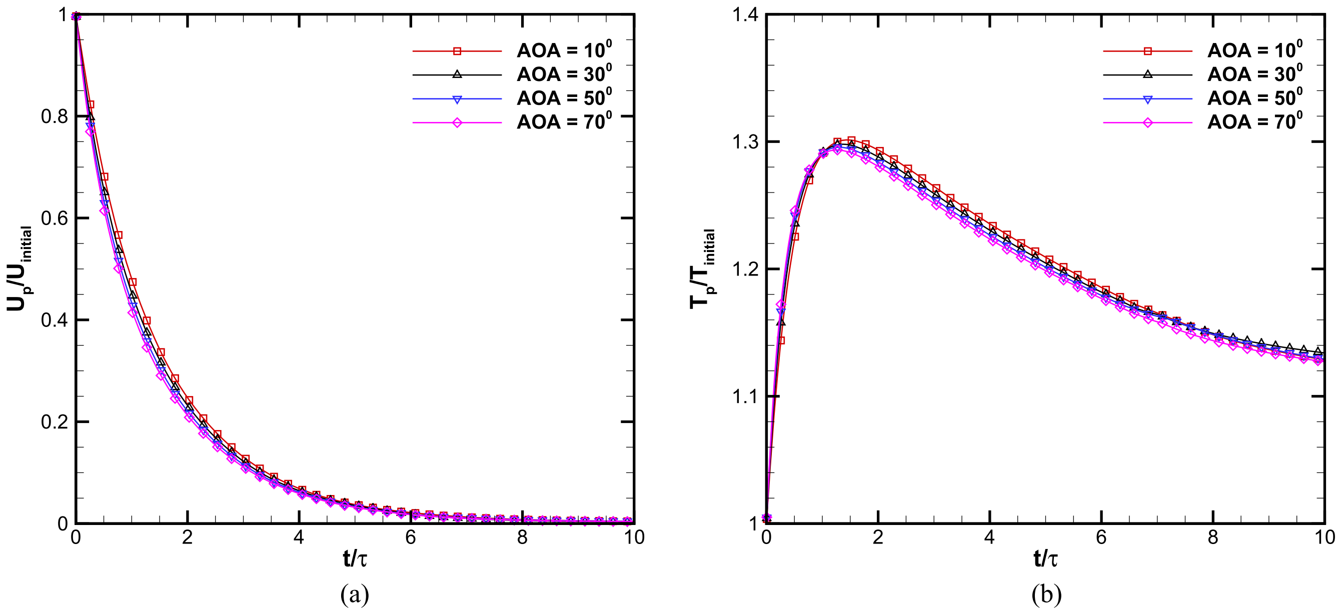

FIG. 17. Comparison of relaxation of a spherical particle with an ellipsoidal for different initial angles of attack (m_p = 9.958 × 10^{-13} kg). (a) Particle speed and (b) particle temperature.

not found to be significant in this work. Furthermore, the difference in the lift coefficient between DSMC and continuum theory is visibly sufficiently high. However, the theoretical lift coefficient relation given in Eq. (24) gives an error of 15% for prolate and 60% for oblate spheroids in the continuum regime itself in the work of Sanjeevi and Padding.[39] Moreover, it was observed in the work of Sanjeevi and Padding[39] that the variation of C_L is much more sensitive to the angle of attack than that of C_D.

3. At different initial angles of attack

To study the effect of initial angle of attack, we have simulated ellipsoidal particle relaxation for different initial angles of attack. The flow conditions are the same as that of the previous case. In order to show the effect of initial angle of attack, ellipsoidal eccentricity is chosen as 0.9, while the initial angle of attack is varied from 10 to 80. Figure 17 shows the velocity and thermal relaxation of an ellipsoidal particle at different angles of attack. It is observed that the relaxation time decreases slightly as the initial angle of attack increases although the difference remains less than 10%. The trend observed in speed is found to be the same in temperature as well.

4. Comparison of particle trajectories

The trajectories of ellipsoidal particles of different eccentricity values are compared with spherical particles for an equivalent particle size of 1 μm in Fig. 18. The horizontal distance (x-distance) traveled by individual particles is found to decrease with the increase in particle eccentricity. This is because a particle of larger eccentricity encounters more drag as explained in detail in Sec. IV D 1. It is evident from the figure that the x-distance traveled by particles of different eccentricities is very different, and this is a very important result. On the other hand, the vertical distance traveled by different eccentricity particles is found to be negligibly small, which is the same as that of a sphere. Since this study is performed in the very low-density environment with the diffuse wall condition and very small particle size, the lift force generated by individual particles is very small (as discussed in Sec. IV D 2) and therefore does not play a significant role in altering the trajectory.

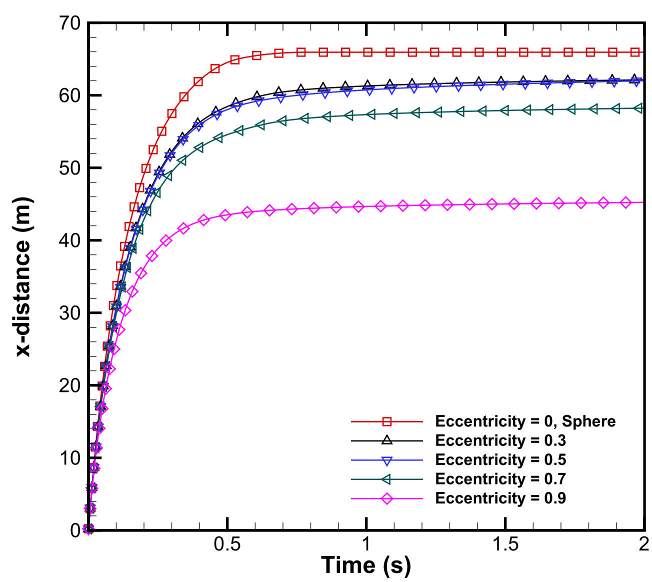

FIG. 18. Comparison of trajectories (x coordinate) of spherical and ellipsoidal particles of different eccentricities.

TABLE I. Important findings.

Parameter	Observations from the present study
Relaxation time	The relaxation time for the ellipsoidal particle was found to increase with eccentricity for zero angle of attack, whereas it behaved the opposite at non-zero angles of attack
Scaling of relaxation time with particle size	The relaxation time for spherical and ellipsoidal particles was found to scale with the equivalent particle diameter in the free molecular regime. This observation was found to be in line with the theory applicable in the free molecular regime for a spherical particle. Noteworthy is the fact that the relaxation time varies proportional to the square of particle diameter in the continuum regime (Kn → 0)
Sensitivity to initial angle of attack	The relaxation time was found to decrease with an increase in the initial angle of attack. It was found that initial orientation of particle is important in calculating particle dynamics accurately
Rotational relaxation	The rotational relaxation time was found to decrease with an increase in eccentricity. It was found that the consideration of rotational particle dynamics is important
Lift coefficient	It was found that the effect of lift on particle dynamics is not important because of the presence of large degree of rarefaction in the present work
Trajectory of particles	The horizontal distance traveled by particles was observed to decrease with an increase in eccentricity. Also noteworthy is the fact that an ellipsoidal particle was found to undergo a very different trajectory as compared to that of a spherical particle, which makes the consideration of particle shape important

Thus it is clear that an ellipsoidal particle undergoes a very different trajectory as compared to a spherical particle in the free molecular regime. This in turn renders the consideration of particle shape effects very important in planetary landing applications and beyond.

V. IMPORTANT FINDINGS OF THE WORK

In the present work, we have developed a computer model to clearly bring out the effects of particle size, shape, and orientation on the transport of a single particle in the free molecular flow regime. In doing so, we have also incorporated the effects of rotational dynamics of non-spherical particles. A few salient findings of this work are presented in Table I.

VI. CONCLUSIONS

The size, shape, and orientation effects of a transporting granular particle in the free molecular gas flow regime were studied using the in-house direct simulation Monte Carlo framework. The same was modified to reduce computational time in the free molecular regime and validated with available analytical results for relaxation of a spherical particle to surrounding gas conditions. Moreover, relaxation of an ellipsoidal particle was studied for different eccentricities and compared with that of a spherical particle. It was found that relaxation time increases with increasing eccentricities at zero angle of attack. On the other hand, interestingly, the same was noticed to decrease for non-zero angles of attack. On the other hand, the effect of lift on particle dynamics was found to be insignificant. The effect of particle size was also studied, and the relaxation time was found to scale with the particle diameter, a result consistent with the theory. Particles of different eccentricities were also compared in terms of their trajectories, and it was found that an ellipsoidal particle can undergo a very different trajectory as compared to that of a sphere, thus making the consideration of particle shape very important. Finally, we studied relaxation of an ellipsoidal particle at different initial angles of attack for a particular eccentricity of 0.9. The relaxation time was found to decrease as the initial angle of attack increased. Therefore, size, shape, and orientation were found to play an important role in governing particle dynamics in the free molecular regime.

ACKNOWLEDGMENTS

We acknowledge the use of the computing facility available at the High Performance Computing Facility of the Computer Centre, IIT Kanpur, India, for carrying out most of the computations associated with this work. R.K. acknowledges the financial support from the Indian Space Research Organization, India, through the Grant No. STC/AE/2018033. R.S.M. acknowledges the support from the National Research Foundation of Korea (No. NRF 2017-R1A2B2007634), South Korea.

REFERENCES

[1] P. S. Epstein, "On the resistance experienced by spheres in their motion through gases," Phys. Rev. **23**(6), 710–733 (1924).
[2] M. J. Baines, I. P. Williams, A. S. Asebiomo, and R. L. Agacy, "Resistance to the motion of a small sphere moving through a gas," Mon. Not. R. Astron. Soc. **130**(1), 63–74 (1965).
[3] F. M. Sauer, "Convective heat transfer from spheres in a free-molecule flow," J. Aeronaut. Sci. **18**(5), 353–354 (1951).

[4]M. A. Gallis, J. R. Torczynski, and D. J. Rader, "An approach for simulating the transport of spherical particles in a rarefied gas flow via the direct simulation Monte Carlo method," Phys. Fluids **13**(11), 3482–3492 (2001).
[5]J. M. Burt, "Monte-Carlo simulation of solid rocket exhaust plumes at high altitude," Ph.D. dissertation (The University of Michigan, 2006).
[6]A. B. Morris, D. B. Goldstein, P. L. Varghese, and L. M. Trafton, "Approach for modeling rocket plume impingement and dust dispersal on the moon," J. Spacecr. Rockets **52**(2), 362–374 (2015).
[7]Z. Li and W. Hai, "Drag force, diffusion coefficient, and electric mobility of small particles. I. Theory applicable to the free-molecule regime," Phys. Rev. E **68**(6), 061206 (2003).
[8]Z. Li and W. Hai, "Drag force, diffusion coefficient, and electric mobility of small particles. II. Application," Phys. Rev. E **68**(6), 061207 (2003).
[9]S. A. Beresnev, V. G. Chernyak, and G. A. Fomyagin, "Motion of a spherical particle in a rarefied gas. Part 2. Drag and thermal polarization," J. Fluid Mech. **219**, 405–421 (1990).
[10]M. Zastawny, G. Mallouppas, F. Zhao, and B. V. Wachem, "Derivation of drag and lift force and torque coefficients for non-spherical particles in flows," Int. J. Multiphase Flow **39**, 227–239 (2012).
[11]O. Rafik, M. Khalij, A. Taniere, and B. Arcen, "Drag, lift and torque coefficients for ellipsoidal particles: From low to moderate particle Reynolds numbers," Comput. Fluids **113**, 53–64 (2015).
[12]G. B. Jeffery, "The motion of ellipsoidal particles immersed in a viscous fluid," Proc. R. Soc. A **102**(715), 161–179 (1922).
[13]G. I. Taylor, "The motion of ellipsoidal particles in a viscous fluid," Proc. R. Soc. A **103**(720), 58–61 (1923).
[14]H. Brenner, "The Stokes resistance of an arbitrary particle," Chem. Eng. Sci. **18**(1), 1–25 (1963).
[15]H. Brenner, "The Stokes resistance of an arbitrary particle—II: An extension," Chem. Eng. Sci. **19**(9), 599–629 (1964).
[16]H. Brenner, "The Stokes resistance of an arbitrary particle—III: Shear fields," Chem. Eng. Sci. **19**(9), 631–651 (1964).
[17]H. Brenner, "The Stokes resistance of an arbitrary particle—IV: Arbitrary fields of flow," Chem. Eng. Sci. **19**(10), 703–727 (1964).
[18]H. Brenner, "The Stokes resistance of an arbitrary particle—Part V: Symbolic operator representation of intrinsic resistance," Chem. Eng. Sci. **21**(1), 97–109 (1966).
[19]P. H. Mortensen, H. I. Andersson, J. J. J. Gillissen, and B. J. Boersma, "Dynamics of prolate ellipsoidal particles in a turbulent channel flow," Phys. Fluids **20**(9), 093302 (2008).
[20]J. Lin, X. Shi, and Z. Yu, "The motion of fibers in an evolving mixing layer," Int. J. Multiphase Flow **29**(8), 1355–1372 (2003).
[21]M. Shapiro and M. Goldenberg, "Deposition of glass fiber particles from turbulent air flow in a pipe," J. Aerosol Sci. **24**(1), 65–87 (1993).
[22]J. D. Klett, "Orientation model for particles in turbulence," J. Atmos. Sci. **52**(12), 2276–2285 (1995).
[23]G. A. Bird, *Molecular Gas Dynamics and Direct Simulation of Gas Flows* (Clarendon Press, Oxford, 1994), p. 508.
[24]P. S. Prasanth and J. K. Kakkassery, "Direct simulation Monte Carlo (DSMC): A numerical method for transition-regime flows-A review," J. Indian Inst. Sci. **86**(3), 169–192 (2013).
[25]R. Kumar and A. K. Chinnappan, "Development of a multi-species, parallel, 3D direct simulation Monte-Carlo solver for rarefied gas flows," Comput. Fluids **159**, 204–216 (2017).
[26]A. K. Chinnappan, G. Malaikannan, and R. Kumar, "Insights into flow and heat transfer aspects of hypersonic rarefied flow over a blunt body with aerospike using direct simulation Monte-Carlo approach," Aerosp. Sci. Technol. **66**, 119–128 (2017).
[27]J. C. Maxwell, "VII. On stresses in rarified gases arising from inequalities of temperature," Philos. Trans. R. Soc. London **170**, 231–256 (1879).
[28]J. F. Padilla and I. D. Boyd, "Assessment of gas-surface interaction models for computation of rarefied hypersonic flow," J. Thermophys. Heat Transfer **23**(1), 96–105 (2009).
[29]P. A. Chambre and S. A. Schaaf, *Flow of Rarefied Gases* (Princeton University Press, 2017), Vol. 4971.
[30]A. K. Oppenheim, "Generalized theory of convective heat transfer in a free-molecule flow," J. Aeronaut. Sci. **20**(1), 49–58 (1953).
[31]F. G. Fan and G. Ahmadi, "Wall deposition of small ellipsoids from turbulent air flows—A Brownian dynamics simulation," J. Aerosol Sci. **31**(10), 1205–1229 (2000).
[32]M. Mandø and L. Rosendahl, "On the motion of non-spherical particles at high Reynolds number," Powder Technol. **202**(1-3), 1–13 (2010).
[33]L. Rosendahl, "Using a multi-parameter particle shape description to predict the motion of non-spherical particle shapes in swirling flow," Appl. Math. Modell. **24**(1), 11–25 (2000).
[34]C. Yin, L. Rosendahl, S. K. Knudsen, and H. Srensen, "Modelling the motion of cylindrical particles in a nonuniform flow," Chem. Eng. Sci. **58**(15), 3489–3498 (2003).
[35]R. A. Millikan, "The general law of fall of a small spherical body through a gas, and its bearing upon the nature of molecular reflection from surfaces," Phys. Rev. **22**(1), 1–23 (1923).
[36]M. C. Celenligil, J. N. Moss, and R. C. Blanchard, "Three-dimensional rarefied flow simulations for the aeroassist flight experiment vehicle," AIAA J. **29**(1), 52–57 (1991).
[37]J. N. Moss, C. E. Glass, and F. A. Greene, "Blunt body aerodynamics for hypersonic low density flows," in *Proceedings of 25th Symposium on Rarefied Gas Dynamics* (Publishing House of Siberian Branch of the Russian Academy of Sciences, 2006), Vol. 1, pp. 753–758.
[38]J. Happel and H. Brenner, *Low Reynolds Number Hydrodynamics: With Special Applications to Particulate Media* (Springer Science & Business Media, 2012), Vol. 1.
[39]S. K. P. Sanjeevi and J. T. Padding, "On the orientational dependence of drag experienced by spheroids," J. Fluid Mech. **820**, R1 (2017).